

LIFE PREDICTION ANALYSIS OF THICK ADHESIVE BOND LINES UNDER VARIABLE AMPLITUDE FATIGUE LOADING

Alexandros E. Antoniou¹, Merle M. Vespermann¹, Florian Sayer¹ and Alexander Krimmer²

¹Fraunhofer IWES Institute for Wind Energy Systems, Rotor Blade Department, Am Seedeich 45,
27572 Bremerhaven, Germany

Email: alexandros.antoniou@iwes.fraunhofer.de, Web Page: [http:// www.iwes.fraunhofer.de](http://www.iwes.fraunhofer.de)

Email: merle.vesperman@gmail.com

Email: florian.sayer@iwes.fraunhofer.de, Web Page: [http:// www.iwes.fraunhofer.de](http://www.iwes.fraunhofer.de)

²EUROS GmbH, Materials Department, Falkenberger Straße 146 A/B, 13088 Berlin, Germany

Email: alexander@krimmer-berlin.de, Web Page: [http:// www.euros. de](http://www.euros.de)

Keywords: composite joint, variable amplitude, fatigue, life prediction, thick adhesive

Abstract

Wind turbine rotor blades are exposed to arbitrary wind loadings and consequently their adhesive bond lines along the blade span. Residual stresses, developed due to the manufacturing curing process, are superimposed as steady state components on the wind loadings, shifting the fatigue stress ratios apart from the external imposed load ratios. The prediction of the cohesive failure of the adhesive (transverse to the blade length) is of vital importance since it could propagate in the adjacent laminates, leading potentially into catastrophic failures. A prediction method is proposed regarding the crack initiation and is validated in the adhesive bond line of a generic structural element. The modular method is based on a Goodman diagram and a linear damage accumulation rule. Thus, a generic composite I-beam adhesive joint was designed and manufactured, mimicking the axial-to-shear stress ratio in the bond line between spar caps and shear web of a MW scale wind turbine blade. This was tested under asymmetric three point bending, under static and fatigue variable amplitude loading. The manufacturing residual stresses were calculated analytically based on raw experimental data.

1. Introduction

Wind turbine rotor blades are exposed to varying wind loads, which are inducing fatigue stresses in different R ratios for all the implemented materials. These are design drivers especially for the large offshore structures [1]. Besides that, the blades manufacturing process can result in residual stresses, especially for polymers, which are superimposed to the fatigue stresses as steady state effects. Epoxy based adhesives are widely used in the blade manufacturing as a cost effective solution with good manufacturing and mechanical properties. Thick adhesive bond lines can be found in large structures where manufacturing tolerances are compensated. In the case of wind turbine blades e.g. in the blind bond line between shear webs and the spar caps, thicknesses can range between 5 and 20mm.

Epoxy adhesives are reacting exothermally. Depending on the curing cycle and the applied material volume the exothermal peak might vary. Thus, they are deforming due to their thermal expansion factor. Simultaneously, a chemical shrinkage process is taking place, depending on the degree of curing. The difference of the thermal expansion factor between the adhesive material and the adjacent substrates is resulting in residual steady state strains [2]. These are laid over on the strains developed due to the chemical shrinkage. In the current study relaxation effects were neglected.

In state-of-the-art guidelines for wind turbine blades [3], towards the adhesive joint design verification for a life-span of at least twenty years, several damage modes are considered. Amongst others, it is recommended that the bond line should be designed against cohesive failure. Therefore, besides other stress components, shear and axial stress limits derived from demonstrated tests have to be considered. For the corresponding fatigue analysis, a stress-life approach is advised based on reliable experimental S/N data. Moreover, it is also stated that the adhesive joints are strongly dependent on the bond line thickness and therefore the characteristic strength of the materials have to be reduced by safety factors.

The most common models found in literature for the fatigue design of bond lines subjected under arbitrary fatigue loads are based on an analysis methodology as described in [4]. The first step of the analysis procedure is to deconvolute the load time series into well-defined fatigue load sinusoidal cycles with the Rainflow counting method [5]. The corresponding load and thus the amplitudes and mean stresses are summarized in a Markov matrix. The accumulated damage is calculated with the linear Palmgren-Miner rule [6-7] based on an engineering approach for the allowable fatigue cycles for each R ratio and stress level, e.g. Goodman [8].

In the current proposed modelling sequence, the same modular analysis is implemented focused on the prediction of the bond line cohesive failure under the combination of uniaxial and shear stress components. Moreover, the residual stresses induced due to the curing cycle and the adhesive exothermal reaction are considered in the overall stress calculations. A modified Goodman criterion is implemented for the prediction of the adhesive fatigue resistance to cohesive failure, established on limited experimental data as proposed in [9].

A generic beam element was designed [10], emulating the bond line axial to shear stress ratio of a MW scale wind turbine blade. It was used for benchmarking the analysis results. This was manufactured in the laboratory under temperature-controlled environment and tested under asymmetric three point bending both static and variable fatigue loading. Two different variable amplitude time series were applied experimentally as described in [11] and for the corresponding fatigue analysis.

2. Description of modular fatigue damage model

A fatigue analysis tool was developed consisting of the following modules, as described in Figure 1.

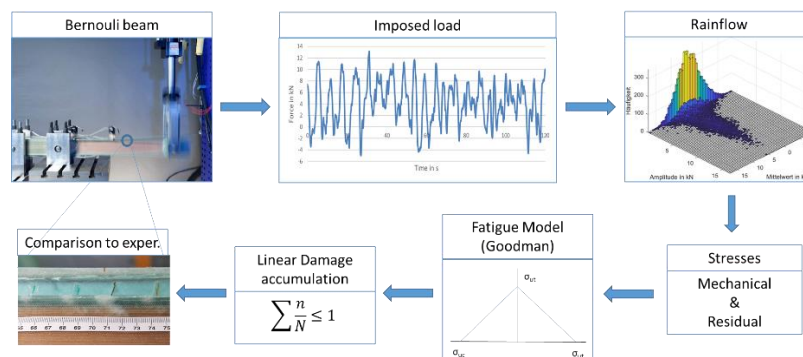


Figure 1. Analysis method for modeling

The two-parametric rainflow method [5] was facilitating the deconvolution of the imposed arbitrary external loads into a number of classes (bins) for the corresponding amplitudes and mean loads of the spectrum. The resulting Markov Matrix (64x64), was also summarizing the respective number of cycles for every class. Therefore, a MATLAB routine was implemented, created by A. Nieslony [12] according

to the standard procedure described in [5]. The analyses of both load time series are shown in Figure 2, as three dimensional bar charts. They both look very similar, whereby series No. 2 consisted of more cycles in classes with high amplitudes. Given that the load \pm signal indicates different direction of the external imposed load, one bond line of the generic beam structure was loaded more in tension rather than in compression. The time of the cycle occurrence and their period were neglected.

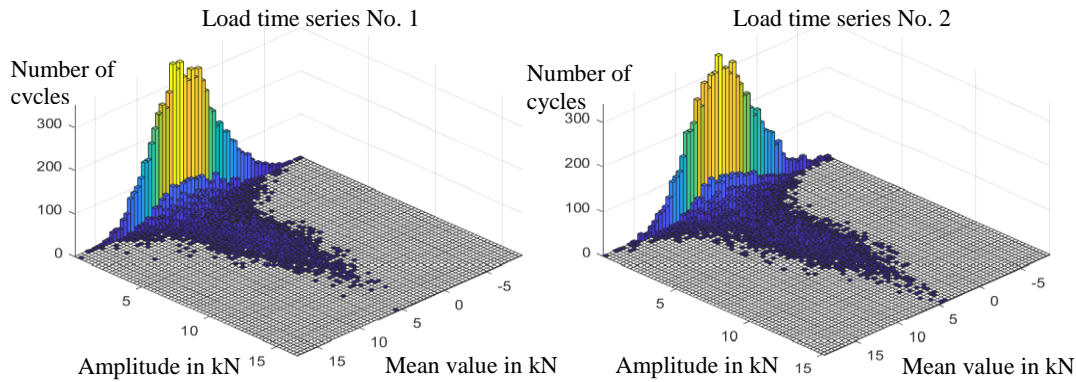


Figure 2. Results from the Rainflow Counting for two different load time series

The corresponding mechanical stresses developed in the bond line were derived through a semi-analytical Euler-Bernouli beam model [13]. A simplified biaxial stress state was assumed, taking under consideration the superposition of the axial and the shear stress components along the bond line length. The beam geometry and construction details are shown in Figure 3.

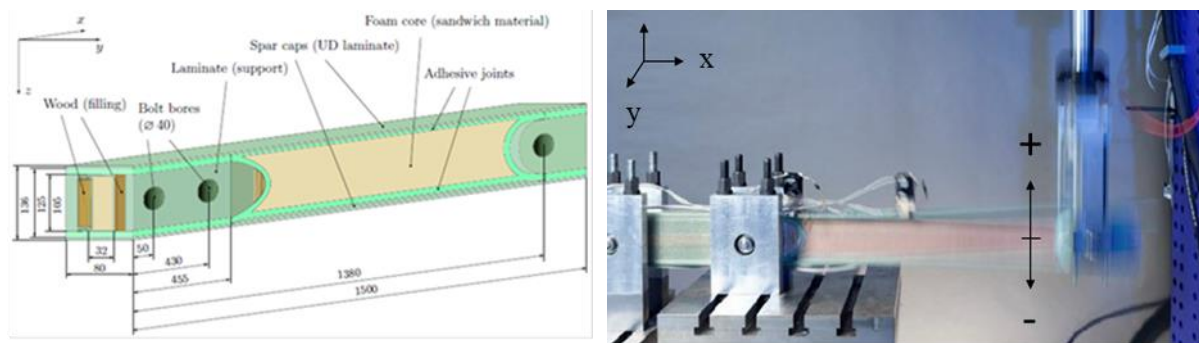


Figure 3. Left: Beam geometry and construction details, Right: Beam test configuration

The residual stresses (σ_{RS}^{Tot}) induced through the manufacturing process were determined under the following hypotheses, a. that there is no relaxation effects, b. that the bond line is almost fully cured i.e. 95% degree of curing and c. that residual stresses consist of a thermal (σ_{RS}^{Therm}) and a chemical part (σ_{RS}^{Chem}) and d. that the adhesive was shrinking uniformly along and transverse to the beam length (x - y plane). The shrinkage in through the thickness z -direction was neglected. Moreover, due to the fact that the spar-cap and the shear web laminates had a thermal expansion coefficient at least one order of magnitude lower than the adhesive material, the substrates were considered as non-deformable with the temperature. This led to a conservative residual stress prediction. Given a linear-elastic performance of the adhesive, with an elastic modulus E_A and a Poisson ratio ν_A , the bond-line residual stresses were derived based on Eq. (1):

$$\sigma_{RS} = \frac{E_A \cdot \varepsilon}{1 - \nu_A} \quad \text{and} \quad \varepsilon = \alpha_A \cdot \Delta T \quad (1)$$

Two scenarios were implemented for the calculation of the thermal residual stresses. The first was based on an incremental stress development assumption, and their accumulation during the cooling phase of the curing cycle. At the same time the adhesive material elastic modulus E_A and its Poisson ratio ν_A were depending on the bond line temperature. These incremental stress steps are described below:

$$\Delta\sigma_{RS}^{\text{Therm.}} = \frac{E_A(T_i) \cdot \Delta\varepsilon_i}{1 - \nu_A(T_i)} \quad \text{and} \quad \Delta\varepsilon_i = \alpha_A \cdot \Delta T_i \quad (2)$$

The temperature dependent material properties [14] are shown in Figure 4.

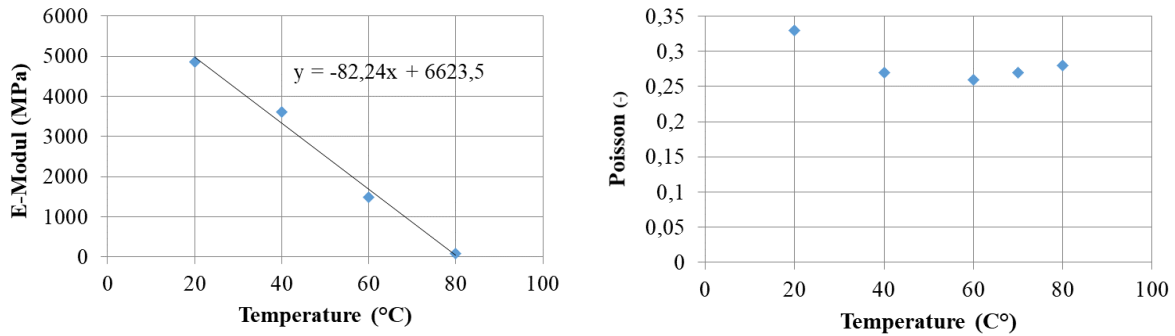


Figure 4. Left: E-Modul vs. Temperature, Right: Poisson ratio vs. Temperature

Based on an internal test campaign [15], the thermal expansion factor value between room temperature and $T = 54^\circ\text{C}$ had a value of $\alpha_{A1} = 26,79 \cdot 10^{-6} \text{ K}^{-1}$, while at higher temperatures had a value of $\alpha_{A2} = 95,10 \cdot 10^{-6} \text{ K}^{-1}$. The intergration of the incremental stresses over the cooling phase of the curing cycle, resulted into thermal residual stresses of $\sigma_{RS1}^{\text{Therm.}} = 10,2 \text{ MPa}$. In the alternative scenario, the cummulative residual strain value acted directly on the cured material with a modulus of Elasticity E_A of 4,5 GPa. The correponding stresses were calculated $\sigma_{RS2}^{\text{Therm.}} = 16,41 \text{ MPa}$.

According to the adhesive material commercial datasheet [16] the volumetric shrinkage was 4.16%. One-third of the total volumetric shrinkage corresponds to linear-axial shrinkage. It was also supposed that the gelation of the adhesive started after 50% of curing degree [17], which means that the rest 50% was responsible for the development of the residual strains. Assuming that the residual strains act on the cured material, the corresponding chemical stresses were $\sigma_{RS}^{\text{Chem.}} = 0,9 \text{ MPa}$, Eq.(1). This is also a conservative approach since the Young's Modulus of the adhesive is dependent on the temperature and thus the final stress level will be lower.

For the derivation of the fatigue allowable cycle number for all possible R ratios, amplitude and mean stresses, i.e. for the prediction of the bond line transverse cracking initiation, the proposed model from Krimmer et al [9] was implemented. The stresses were expressed in terms of stress effort [18], Eq. (3).

$$e = \frac{\sigma}{R_t} \quad (3)$$

where σ is the equivalent axial stress of the adhesive and R_t the material maximum quasi-static resistance. The equivalent stress was calculated through the von Mises formulation [19]:

$$\sigma = \sqrt{\frac{1}{2} [\sigma_x^2 + \sigma_y^2 + \sigma_z^2 - \sigma_x\sigma_y - \sigma_x\sigma_z - \sigma_y\sigma_z + 3(\tau_{xy}^2 + \tau_{xz}^2 + \tau_{yz}^2)]} \quad (4)$$

It has to be noted that the cohesive failure prediction is performed only for the beam bond line which was mostly loaded under tension. Compressive stresses were also present but their contribution to damage was very small.

The only non zero components in Eq.(4) were the in plane shear τ_{xy} and the total axial stress σ_x . The total axial stress was calculated according to Eq. (5).

$$\sigma_x = \sigma_{\text{mech.}} + \sigma_{\text{RS}}^{\text{Therm.}} + \sigma_{\text{RS}}^{\text{Chem.}} \quad (5)$$

For a given load spectrum i , the effort e_{im} or e_{ia} is the ratio between the mean stress σ_m and the amplitude stress σ_a with the maximum allowable stress R_t respectively.

$$e_{im} = \frac{\sigma_m}{R_t} \quad \text{and} \quad e_{ia} = \frac{\sigma_a}{R_t} \quad (6)$$

The corresponding maximum allowable number of cycles N_i for each combination of amplitude and mean value of the rainflow matrix is given by (7):

$$N_i = \left(\frac{1 - e_{im}}{e_{ia}} \right)^m \quad (7)$$

A two parameter optimization fit on the experimental data [20-21] presented in Figure 5, resulted on a set R_t and m parameters which are considered as characteristic for the specific adhesive material.

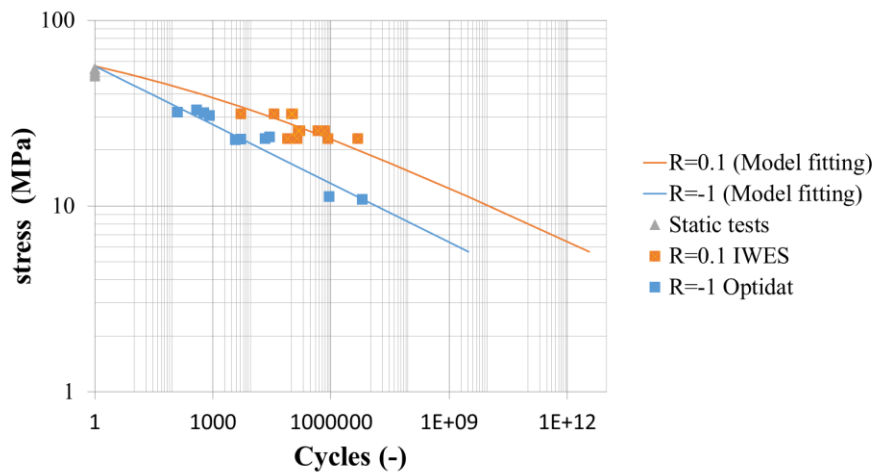


Figure 5. Prediction model fitting.

The Palmgren-Miner rule [6-7] was applied on the Markov matrix to derive the cumulative damage D_i .

$$D = \sum_{i=1}^k \frac{n_i}{N_i} \quad (8)$$

Where n_i was the cycle number derived with the rainflow counting and N_i the allowable number of cycles to damage.

3. Experiment

3.1. Test specimen and manufacturing

The beam was designed as described in [10]. The adhesive bond line between 690-890mm had a constant strain distribution. That was considered as the tested part of the structure, where the cohesive cracks were located. The asymmetric three point bending configuration was statically determined, supported through a roller and a joint support.

The components of the test beam were individually manufactured with the vacuum infusion resin infusion moulding process. The web was designed as a sandwich construction with a foam core. Cover layers and the flanges were made from SAERTEX non-crimped fabric with E-Glass fibres and epoxy resin HEXION RIMR 135 with epoxy hardener RIMH 137. The infusion temperature was 45°C, which was kept constant during the curing process for a duration of eight hours.

Under laboratory conditions the components were bonded with a thermosetting two-component epoxy adhesive, consisting of the adhesive resin HEXION 135G and the hardener 137G, mixed in the material datasheet defined stoichiometric ratio [16], in a planetary mixer. The bond line was applied manually from a cartridge in a thickness of 10mm. Subsequently, the beam was tempered for seven hours at 80°C. Reinforcement plates manufactured of glass fibre composites and plywood were added on both beam ends in the support areas. The beam was tempered again under the aforementioned conditions. The adhesive material temperature was measured during the curing cycle with an encapsulated Pt100.

3.2. Quasi-Static and Variable amplitude fatigue test

All beams were tested quasi-statically before the variable amplitude fatigue loading. Absolute maximum peak and trough values of the implemented time series were applied respectively in the positive and negative directions, as illustrated in Figure 3. The load was introduced at one beam end through a special designed frame that allowed only axial load in the vertical z direction but no bending moment locally.

The variable amplitude load-time series were derived based on the DLC 2.1 [22] calculation and the corresponding bending moments for an 80 m blade [23]. Twenty four-10 minute wind seeds each were generated for the flap wise loadings of the cross section at 25 m and at the wind speed of 21 m/sec. These were combined into a time vector of four hours which was repeated until the catastrophic failure of the beam. The test input force signal was generated from the normalised to unity bending moment vector, multiplied with different weighting load factors for each beam. The test was load controlled.

4. Results and discussion

The cohesive cracks in the bond line of the tested beam are illustrated in Figure 6 (left).



Figure 6. Damage initiation. Left: Vertical cracks in the beam adhesive bond line. Right: Vertical cracks in a WTRB spar to shear web bond line

Their relevance to the wind turbine blades is shown in the the same Figure (right) where a full-scale spar to shear web connection of a tested blade is illustrated with the corresponding bond line cracks.

The results of the proposed modular tool concerning the prediction of the crack initiation are listed in Table 1. Three different scenarios are summarized, two with the different values of the residual stresses and one without any residual stresses.

Table 1. Resulting crack life time from theor. Calc. (t_{th}) and fatigue tests (t_{exp}), expressed in hours

Time series	Beam No.	t_{th1}	t_{th2}	t_{th3}	t_{exp}	
		(h)	(h)	(h)		
		$\sigma_{RS} = 0 \text{ MPa}$	$\sigma_{RS1} = 11.1 \text{ MPa}$	$\sigma_{RS2} = 17.31 \text{ MPa}$		
01	003	35.17	2.74	0.57	9.0	
01	005	1091.33	100.30	21.96	41.0	
01	007	94.01	7.15	0	1.3	
01	009	218.08	21.83	2.96	1.5	
02	004	34.89	2.77	0.32	N/A	
02	006	1027.14	97.74	22.51	96.0	
02	008	91.80	7.87	1.59	5.3	
02	010	209.86	18.78	4.14	1.5	

In Figure 7 is illustrated the maximum test force vs. time of the cohesive crack occurrence. The prediction of the cohesive damage initiation without considering any residual stresses was 1-3 orders of time magnitude offset in comparison to the experimental results of time series 01 pattern. The same is valid for time series 02. Encountering of the residual stresses was resulting to the reduction of the discrepancy down to one order of magnitude. The scatter has to be further investigated. It could be addressed to imperfections due the manual manufacturing process which, according to previous experience, can result into air trapping in the bond line. The test database has to be substantially extended in order to understand and characterize the effect statistically.

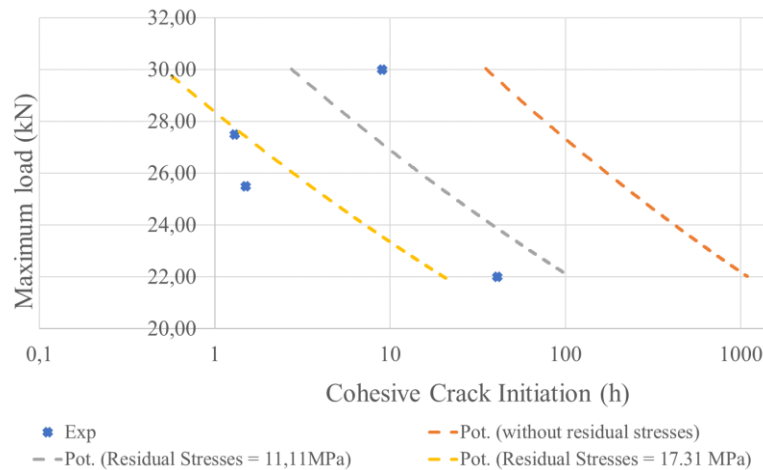


Figure 7. Load time series No. 1: Theoretical and experimental crack life time expressed in hours

5. Conclusions

The contribution of the residual stresses resulting from the manufacturing process are substantial for the prediction of the mechanical performance of thick adhesive bond lines. It was shown that neglecting them can lead to significant errors for the estimation of the fatigue cohesive cracks initiation. The proposed model can analyse the bond line multiaxial fatigue stress states. Its core is the implementation of the residual stresses which are all calculated based on standard experimental data. Moreover, the integrated fatigue damage estimation methodology is based on limited test results. The modular setup of the model enhances the implementation of diverse cycle counting, fatigue and damage accumulation approaches.

Acknowledgments

The current research was performed in the framework of the Intermittente Windlasten (InterWiLa) project granted by the German Federal Ministry for the Environment (BMU) (0325798A)

References

- [1] A. Krimmer. Capabilities of composite materials under fatigue loading. *Proceedings of the IQPC Conference Advances of Blades for Wind Turbines, Bremen, Germany, April 19-21 2016*.
- [2] W. Zhao, K. Ramani. Residual stresses and thermoplastic adhesive environmental cracking. *Proceedings of the 12th International Conference on Composite Materials, Paris, France, 1999*.
- [3] DNVGL-ST-0376. *Rotor blades for wind turbines*. DNV GL AS, 2015.
- [4] Germanischer Lloyd. *Rules and Regulations IV-Non Marine Technology Part 1 Wind Energy*. Germanischer Lloyd, 1993.
- [5] ASTM E1049 – 85. *Standard Practices for Cycle Counting in Fatigue Analysis*, 2017.
- [6] A. Palmgren. Die Lebensdauer von Kugellagern. *Zeitschrift des Vereins Deutscher Ingenieure*, 68:339–341, 1924.
- [7] M.A. Miner. Cumulative damage in fatigue. *J.Appl.Mech*, 12:A159-A164, 1945
- [8] J. Goodman. *Mechanics applied to engineering*. Longman, Green & Company, London, 1899.
- [9] A. Krimmer, A. Antoniou, F. Sayer. Determination and validation of material properties of adhesives for wind turbine blades. *Journal Paper under construction*
- [10] F. Sayer, A. Antoniou, A., van Wingerde. Investigation of structural bond lines in wind turbine blades by sub-component tests. *International Journal of Adhesion and Adhesives*, 37:129–135, 2012.
- [11] W. Popko, M. Wachter, P. Thomas. Verification of Continues Random Time Walk Wind model. *Proceedings of the Twenty-sixth ISOPE International Ocean and Polar Engineering Conference, Rhodes, Greece, June 26 - July 2, 2016*.
- [12] A. Nieslony. *Rainflow Counting Algorithm*, URL: <https://de.mathworks.com/matlabcentral/fileexchange/3026-rainflow-counting-algorithm>, accessed April 27 2018.
- [13] S. Timoschenko, *History of strength of materials*, McGraw-Hill New York, 1953.
- [14] A. Antoniou, F. Sayer, C. Nagel, R. Knaack, P. Wang. *Entwicklung eines Verfahrens zur Bewertung der Betriebsfestigkeit von Blattschalenklebungen für Offshore-Windenergieanlagen (Bladebond)*. Fraunhofer-Institut für Fertigungstechnik und Angewandte Materialforschung, 2013.
- [15] L.Schwab. *Bericht über Applikationsmessungen: Thermomechanische Untersuchungen*, Fraunhofer IWES internal report, 2018
- [16] Hexion GmbH, *Epikote Resin MGS BPR 135G-Series and Epikure Curing Agent MGS BPH 134G-137G*, Technical Data Sheet, 2018
- [17] W.M. Nielsen, *Prediction of process induced shape distortion and residual stresses in large fibre reinforced composite laminates – With application to Wind Turbine Blades*, Ph. D. Dissertation, DTU, 2012
- [18] A. Puck. *Festigkeitsanalyse von Faser-Matrix-Laminaten: Modelle für die Praxis*, Hanser, 1996.
- [19] R. von Mises. Mechanik der festen Körper im plastisch deformablen Zustand. *Göttin. Nachr. Math. Phys.*, 1:582–592, 1913.
- [20] A. Antoniou. *Mechanical characterization of Epikote BRP135 G3*, Internal number 104566_001, IWES Internal report, 2014
- [21] R. Nijssen, *OptiDat Database*, Knowledge Centre WMC, http://www.wmc.eu/optimatblades_optidat.php, accessed Mai 17, 2017
- [22] IEC 61400-1, Wind turbines – Part 1: Design requirements
- [23] A. Sevinc et al., *IWES Wind Turbine IWT-7.5-164*, Technical report, Fraunhofer IWES, 2015